Front. Earth Sci. 2022, 16(4): 975–988
https://doi.org/10.1007/s11707-022-0999-9

RESEARCH ARTICLE

Bedding-parallel fractures in ultradeep tight sandstone reservoirs in Jurassic and Cretaceous of Yongjin Oil Field, Junggar Basin, China

Hongping LIU (✉)[1], Changmin ZHANG (✉)[1], Li ZHANG[1], Yang LUO[2]

1 School of Geosciences, Yangtze University, Wuhan 430100, China
2 Key Laboratory of Tectonics and Petroleum Resources (Ministry of Education), China University of Geosciences, Wuhan 430074, China

Abstract Bedding-parallel fractures are fractures that are parallel to rock bedding structure planes and have been widely accepted as a key factor for oil and gas production in tight sandstone and shale reservoirs. However, the formation mechanisms of these parallel-bedding fractures are still under debate. In this study, bedding-parallel fractures in Yongjin Oil Field were analyzed using methods including core and microscopic observations, element geochemistry, and carbon and oxygen isotope analysis. Their origin and relations to reservoir quality, faults, and rock mechanical properties were examined. The discovery of bedding-parallel fractures in both the Upper Jurassic and Lower Cretaceous formations indicates that the BPFs are generated later than the early Cretaceous. The filling state of bedding-parallel fractures that with no bitumen and carbonate cement indicate that they formed after oil charging and carbonate cementation. The tensile fracture characteristics in core and thin section observations, and the fact that overburden stress exceeds the pore pressure indicate that the bedding-parallel fractures were neither generated from tectonic compression nor overpressure. The most likely generation mechanism is stress relief during core drilling under high in situ stress conditions. High in situ stress and low tensile strength lead to thinner fracture spacing. The existence of high bedding-parallel fracture density is an indicator of good reservoir quality and result in high oil/gas production.

Keywords Bedding-parallel fractures, ultradeep reservoirs, tight sandstone, fracture origin, Junggar Basin

1 Introduction

Bedding-parallel fractures (BPFs) are fractures that are parallel to rock bedding structure planes and have been widely discovered in shale and tight sandstone oil/gas reservoirs (Flottmann et al., 2004; Luo et al., 2017; Su et al., 2022; Zeng et al., 2022), and have also been found to lead to high oil/gas production rates (Wu et al., 2003; He et al., 2011; Luo et al., 2017). Bedding-parallel fractures can either pass through part of the cores or spill into several discs with similar thicknesses that are normal to the axis of the boreholes. The separated discs are usually named "core discing" by geologists (Jaeger and Cook, 1963; Obert and Stephenson, 1965; Hou, 1985; Wu et al., 2003). The discovery of core discing in sandstones dates back to the early 21st century in the Copper Basin, Australia (Flottmann et al., 2004) and tight sandstones of the Sichuan Basin, China (Wu et al., 2003). However, core discing was first observed in the 1950s, and more discoveries by geotechnical engineers proliferated in different lithologies, such as sandstone, granite, and marble (Jaeger and Cook, 1963; Obert and Stephenson, 1965; Hou, 1985).

The origin of BPFs remains different according to petroleum geologists and geotechnical engineers at present. Petroleum geologists attribute BPF origin to factors such as natural hydraulic fracturing (Wu et al., 2003; Zhang and Lan, 2006), tectonic compression (Zeng et al., 2009; He et al., 2011), and tensile fracture caused by overpressure (Luo et al., 2017). The viewpoint of BPF origin among geotechnical engineers is almost the same, which suggests that it is a result of tensile failure at the time of borehole drilling in areas with high horizontal stresses (Jaeger and Cook, 1963; Obert and Stephenson, 1965; Hou, 1985; Lim and Martin, 2010; Zheng et al., 2020).

The debates on the origin of BPFs among petroleum geologists are mainly affected by the complex filling states of the bedding-parallel fractures in sandstone reservoirs and shale (Wu et al., 2003; Flottmann et al.,

Received April 7, 2022; accepted June 7, 2022

E-mail: liuhongping12@126.com (Hongping LIU)
zcm@yangtzeu.edu.cn (Changmin ZHANG)

2004; Cobbold and Rodrigues, 2007; Zeng et al., 2009; Ukar et al., 2017; Li et al., 2021; Su et al., 2022). Previous studies have shown that the BPFs in shale are filled with calcite beef veins (Cobbold and Rodrigues, 2007; Zanella et al., 2015; Ukar et al., 2017; Su et al., 2022; Lai et al., 2022), whereas most BPFs in sandstone (Wu et al., 2003; Zeng et al.,2009; He et al., 2011; Ju et al., 2020) and carbonate reservoirs (Li et al., 2021) are without cement. Calcite beef veins in BPFs of shale usually preserve solid bitumen inclusions and/or liquid oil- or gas-bearing inclusions, which can be used to constrain formation time (Zanella et al., 2015; Zhang et al., 2016; Wang et al., 2020). Recently, new techniques, such as U–Pb dating (Su et al., 2022), have been used to accurately ascertain formation time. The fracture-filling time from different methods demonstrates varying times from before consolidation of the sediments (Su et al., 2022) to formation at the time after oil charging (Zanella et al., 2015; Zhang et al., 2016; Wang et al., 2020). Both results suggest that the opening of the fractures was caused by overpressure that led to natural hydraulic fracturing either by biogenetic gas generation (Su et al., 2022) or oil generation (Zanella et al., 2015; Zhang et al., 2016; Wang et al., 2020).

The lack of cement in BPFs in sandstone and carbonate reservoirs has led to more discussion. Wu et al. (2003) and Ju et al. (2020) believed that the low-dip angle fractures in tight gas sandstones of the Sichuan Basin are bedding fractures that were mainly caused by natural hydraulic fracturing at the time of gas generation. In addition, tectonic uplift after the formation of the bedding fracture led to the opening of the bedding fractures. He et al. (2011) first discovered core discing in the Upper Jurassic tight sandstones in our study area and argued that the intensive tectonic compression after burial formed the BPFs. The continuing charging of oil and gas maintains the opening of the BPFs. Zeng et al. (2009) and Li et al. (2021) described the characteristics of the BPFs and conducted numerical modeling. Their results showed that thrust faults caused by intensive compression may have resulted in BPFs in tight sandstones in the western part of the basins of China. Most previous studies gave the possible origins of the BPFs or core discing. However, much important evidence still does not support these conclusions. The important contradictions include the following. (i) Many of the previous studies emphasized the effects of natural hydraulic fracturing caused by oil/gas generation. However, core descriptions indicated that the BPFs are without cement, which is different from the high-dip angle (HDA) fractures that are filled by calcite (Luo et al., 2020). (ii) Most previous work valued intensive tectonic compression and concluded that the BPFs were shear fractures (Zeng et al., 2009; He et al., 2011; Li et al., 2021). However, no clear evidence in thin sections supports the hypothesis.

In this study, a detailed description of the BPFs on core and microscales in the Jurassic and Cretaceous tight sandstones in the Junggar Basin was performed first. Then, their relationship with lithology, reservoir quality, and tectonic background was analyzed. Some indirect evidence, such as geochemistry and burial history, was also employed to estimate the origin of the BPFs.

2 Geological settings

The Junggar Basin is one of the largest petroliferous basins in north-west China. It is located in Xinjiang and is surrounded by the Zaire Mountains and Halaalate Mountains in the north-west, the Qinggelidi Mountains and Kelameili Mountains in the north-east, and the Yilinheibiergen Mountains and Bogda Mountains in the south (Fig. 1(a)). There are six major tectonic units in the basin, including four major tectonic units, the Wulungu Depression, Luliang Uplift, Central Depression, and Tianshan Foreland, in the middle of the basin (Fig. 1(b)). The other two major tectonic units, the West Uplift and East Uplift, are on the western and eastern edges of the basin, respectively.

The Yongjin Oil Field is located in the center of the Central Depression Unit. The thick sedimentary sequence of the Junggar Basin is underlain by a pre-Carboniferous basement. According to the preferred stratigraphic framework of the Xinjiang Oil Field Company, the post-accretionary sequence of the Junggar Basin is subdivided into 23 lithostratigraphic formations with a maximum total thickness of approximately 14000 m (Bian et al., 2010). The basin fill is subdivided into three tectonically controlled stratigraphic sequences: 1) foreland basin cycle from the Permian to Triassic, 2) intracontinental depression basin cycle from the Jurassic to Paleogene, and 3) reactivated foreland basin cycle in the Neogene.

The oil reservoirs were mainly discovered in the Upper Jurassic Qigu Formation (J_3) with the burial depth ranges from 5500 to 6500 m, which was controlled by a regional unconformity between the Jurassic and Cretaceous (Fig. 2). Due to uplift during the Late Jurassic in the study area, the Toutunhe and Kalaza Formations were all eroded, with the Qigu Formation directly overlying the Xishanyao Formation (Fig. 2). The paleoenvironment changed from humid to dry from the Xishanyao Formation to the Qigu Formation. The sedimentary facies of the study area include a shallow-water delta that stretches from north-west to south-east.

Figure 1(c) shows the structural map of the top of the Upper Jurassic. The erosion of the Jurassic formation was caused by north–south compression during the Yanshanian period and formed thrust faults to the west and east. The thrust faults from the south to the north were formed by Himalayan movements after the Cretaceous with a structural trend of high in the north and low in the south (Qu et al., 2009; Bian et al., 2010).

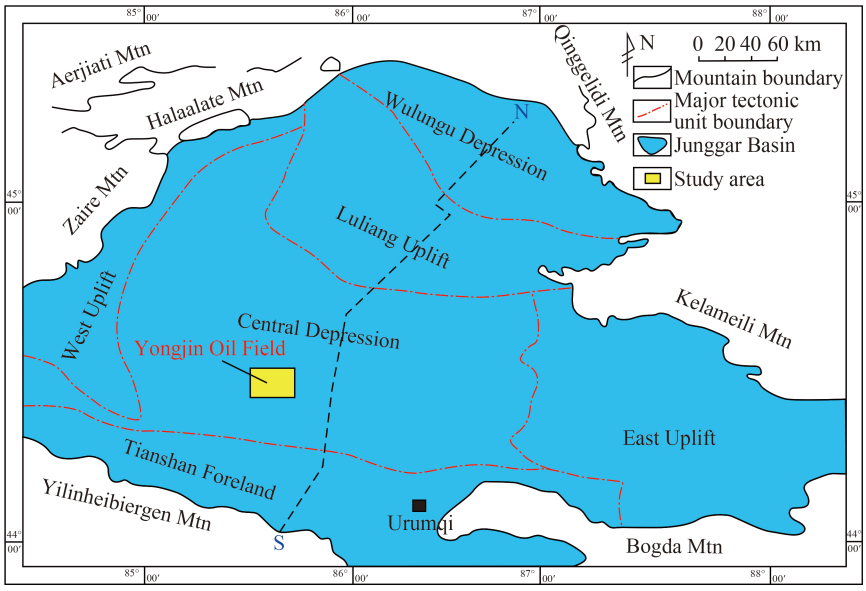

(a)

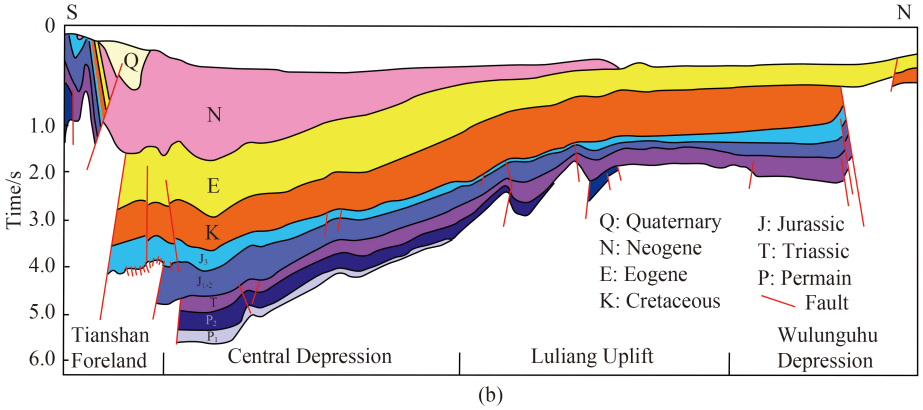

(b)

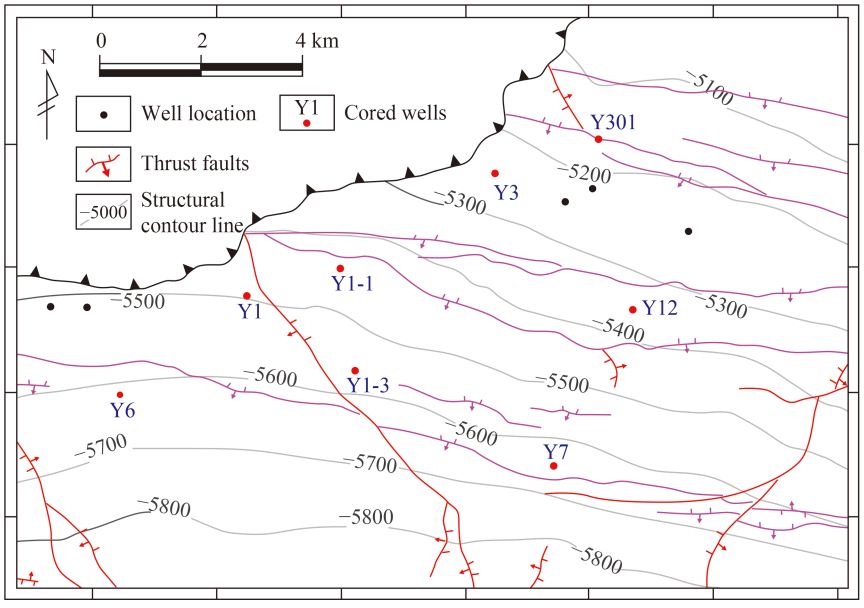

(c)

Fig. 1 (a) Major tectonic units of the Junggar Basin (modified from Bian et al., 2010). (b) Cross-section through the Junggar Basin from south to north (modified from Yang, 2009). (c) Structure image of the top of the Jurassic units.

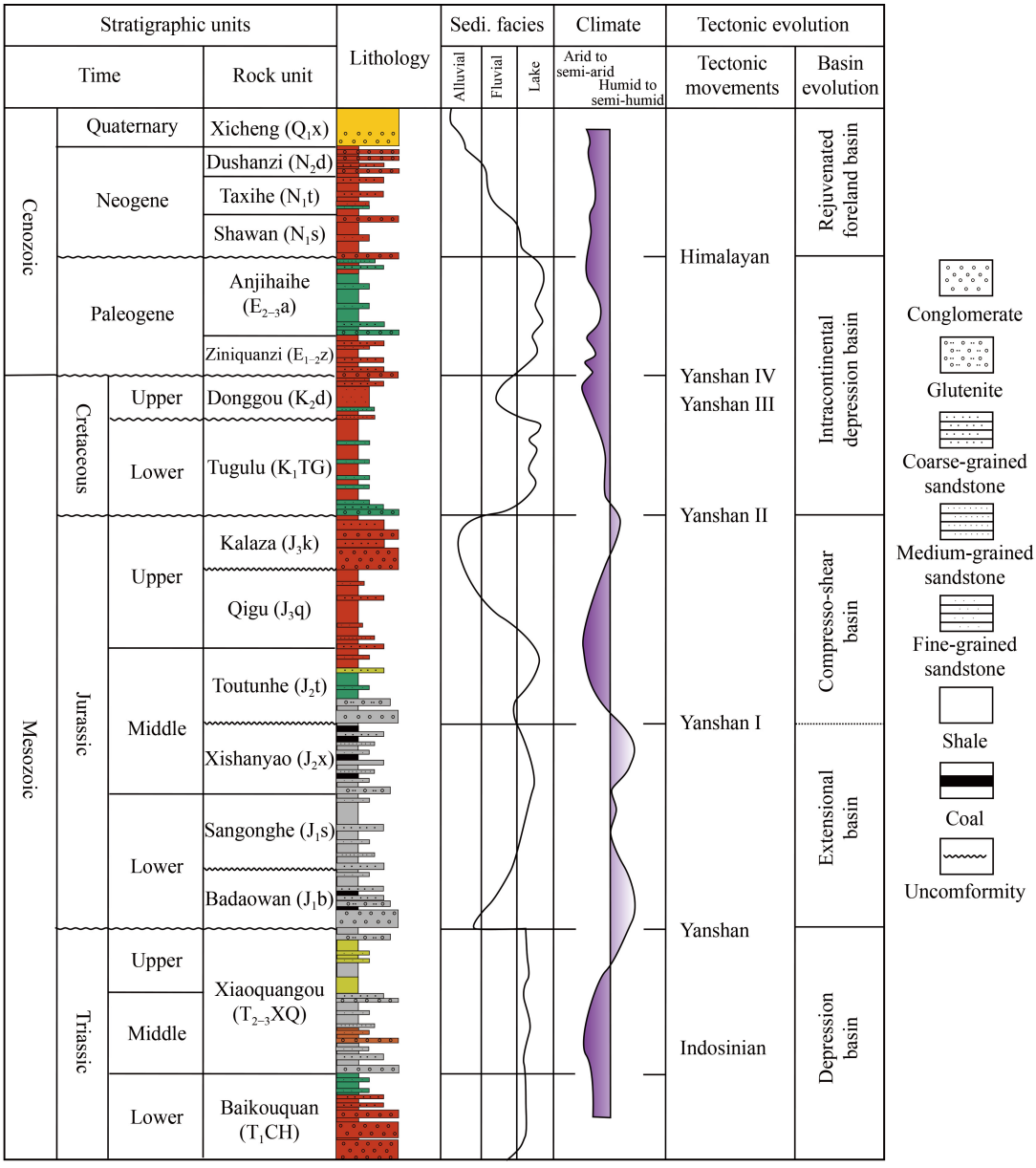

Fig. 2 Stratigraphic names and ages, lithologies, sedimentary environments, and tectonic evolution of the Junggar Basin, China (modified from Hu et al., 2020).

Petroleum system studies showed that the main oil and gas source rocks were shale of middle-late Permian age and coal in the Middle Jurassic Xishanyao Formation (Shi et al., 2009; Yang et al., 2011), respectively. The reservoir is recognized as an ultradeep and overpressured stratigraphic trap oil reservoir, with little gas production. The pressure coefficient mainly ranges from 1.5 to 1.8, which is very high and contributes to the high oil production rate in some of the wells.

3 Data and methods

This study mainly focused on the Upper Jurassic Qigu Formation in the Yongjin Oil Field, Junggar Basin, China. Cores from the Lower Cretaceous formation were also observed and analyzed. In this study, the observations and experiments mainly consisted of three parts, including reservoir properties, fracture characterization, and stable isotope analysis, to constrain the timing of the BPFs. The databases came from 9 cored wells with a total length of approximately 210 m, which are evenly distributed in the study area (Fig. 1(c)). Production data and rock mechanical property data were also collected from the Shengli oil company of SINOPEC.

3.1 Reservoir properties

Reservoir properties include lithology, porosity, permeability, and diagenetic properties of the study area.

Lithology is determined by core observations and thin section analysis. Sixty thin sections were used to analyze the composition of the rocks and diagenetic types, and point counting was performed on thin sections with at least 300 points. Ninety-one samples with a diameter of 2.5 cm and a length of approximately 3−4 cm were used for porosity and permeability analyses. Porosity was measured using a JS100007 helium porosimeter, and permeability was measured using an A-10133 gas permeameter following standard industry methods with a confining pressure of 500 psi and high purity nitrogen of 99.999%.

3.2 Fracture characterization

Fracture characterization includes core observations, thin section analysis, and fracture surface analysis. The fracture density was calculated with a sample spacing of 0.25 m. Sixty thin sections with blue epoxy were used to analyze the fracture occurrence and filling states. The Niton™ XL2 Plus portable element analyzer was used to detect whether there was calcite or quartz cement on the fracture surfaces.

3.3 Carbon and oxygen isotopes

The carbon and oxygen isotope data were used to determine the origin of the carbonate cement and the precipitation temperature. The data may be indirectly used to constrain the formation time of the fractures. Thirty-six sandstone samples were chosen for the carbon and oxygen stable isotope analyses. Samples were disaggregated directly with a hammer and then crushed in a mortar. The disaggregated samples were passed through a 200-mesh sieve (75 mm). The powder samples were heated to 400°C for 4 h to remove any organic compounds. Extracted CO_2 was transferred to a Thermo Fisher MAT253 isotope ratio mass spectrometer for the determination of stable C and O isotope compositions. The analytical errors are below 0.1‰.

4 Results

4.1 Lithology and reservoir quality

The sedimentary facies of the study area include a delta front and delta plain, with medium- to fine-grained sandstones dominating the lithology. Composition analysis shows that feldspathic-litharenite and lithic sandstone are the main lithology types in the Qigu Formation (Fig. 3(a)). The quartz content ranges from 20%−55%, with an average of 29.2%. The feldspar content ranges from 3%−33%, with an average of 18.9%. Lithics are the main grain type, with a content ranging from 28%−91% and an average of 54.1%. The lithic types in the Qigu Formation are mainly composed of volcanic rock fragments and metamorphic rock fragments (Fig. 3(b)). The clay matrix amount is very low in medium- and fine-grained sandstones, which is a result of the long exposure during the Late Jurassic (Hu et al., 2008).

Statistics of the 91 measured porosity and permeability data show that it is a typical tight sandstone reservoir (Fig. 4). The porosity ranges from 4% to 14%, with an average of 7.68%. Permeability shows a much wider range from 0.01 to 4 mD, which indicates the complex rock types in the ultradeep tight sandstones. The real porosity and permeability may be higher than the statistics since the core discing makes it difficult to collect 2.5 cm diameter samples in some of the disc-like cores.

Oil production in the study area also varies, and Wells Y1, Y3, and Y301 show production rates ranging from 20

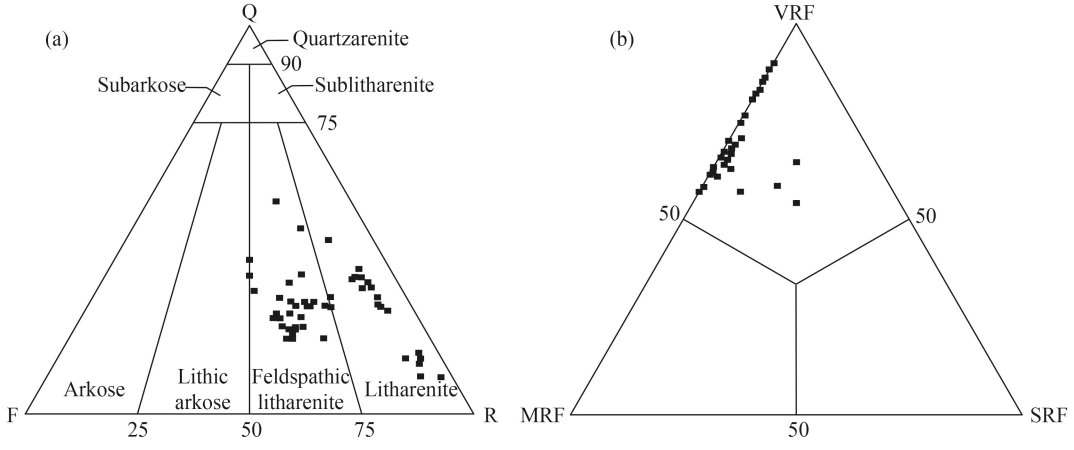

Fig. 3 (a) Ternary diagram illustrating the framework compositions of the Upper Jurassic tight sandstones in the Yongjin Oil Field. Q = quartz; F = feldspar; and R = rock fragment. (b) Rock fragment ternary plot of the Upper Jurassic tight sandstones. VRF = volcanic rock fragments; MRF = metamorphic rock fragments; and SRF = sedimentary rock fragments.

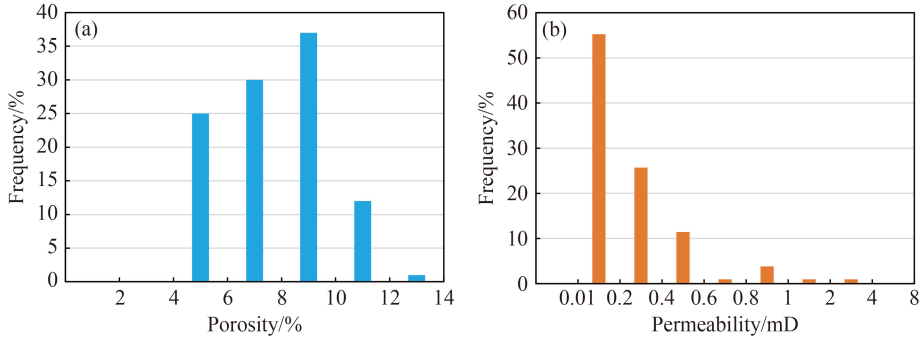

Fig. 4 (a) Porosity and (b) permeability histograms of the Qigu Formation.

to 50 t/day. However, the other cored wells display an oil production rate of less than 1 t/day or almost no oil production.

4.2 Diagenesis

The main diagenesis in the study area included compaction, cementation, and dissolution.

Compaction: Compaction in the study area varies in different rock types. In the fine-grained sandstones and silt, the grain contact type is mainly line contact with only a few dissolution pores (Fig. 5(a)), indicating intensive compaction. However, the line-point contact or point contact dominates the contact type in the medium- to fine-grained sandstones with high contents of quartz (Figs. 5(b) and 5(c)), which implies medium compaction. The pore types in these medium compaction rocks include residual intergranular pores and dissolution pores. Previous studies inferred medium compaction in the ultradeep reservoirs from high overpressure in the study area (Hu et al., 2008; Yang et al., 2011).

Cementation: Cement in the study area mainly includes carbonate, quartz overgrowth, and authigenic clay minerals such as chlorite and kaolinite. Unlike the tight sandstones in the Ordos Basin (Liu et al., 2020; Liu et al., 2021), the sandstones in our study area are rather clean with a very low content of clay matrix and authigenic clay. Many thin sections with abundant pores show very few authigenic clays (Figs. 5(b) and 5(c)). Only a few thin sections show chlorite coats and authigenic kaolinite (Fig. 5(d)). Quartz overgrowths can be widely observed (Fig. 5(e)), but they have a low content, approximately 1.6%. Carbonate cements, including calcite and dolomite, are the main forms of cementation in the study area. Calcite is mainly observed as poikilitic cementation in the intergranular pores (Figs. 5(f) and 5(h)), and dolomite is mainly automorphic and granular with partial dissolution (Fig. 5(g)). The thin sections show that the dolomite cement altered the calcite cement (Fig. 5(h)), which indicates that the dolomite cement formed later than the calcite cement.

Dissolution: Dissolution is a very important mechanism for the formation of sweet spots in the study area. Grain dissolution includes feldspar and lithic dissolution (Fig. 5(i)). In most cases, grain dissolution may preserve authigenic clays. However, since the Late Jurassic reservoir was an open diagenetic environment, most clay minerals were not preserved, which led to the high intergranular pores in the study area (Hu et al., 2008).

4.3 Fracture characterization

4.3.1 Fracture type and distribution in core observations

Fractures can be classified by the dip angle (vertical, high-dip angle, low-dip angle, and bedding parallel), origin (tectonic, diagenetic, and induced fractures), and filling states (filled, unfilled, and partly filled) (Zeng et al., 2007, 2009; Luo et al., 2017). Three types of fractures can be discerned in the study area when classifying the fractures by dip angle (Fig. 6). One type is BPFs, and the other two types are vertical and high-angle fractures, with the BPF being the dominant fracture type. Statistics of cores from 9 wells show that BPFs contribute 97.4% of the total number of fractures. However, vertical and high dip-angle fractures only contribute to 2.6% of the total fractures. The BPF density ranges from 0−50 m^{-1}, with an average of 21.7 m^{-1}. The BPF spacing ranges from 1 cm to 10 cm, which varies from one lithology to another. BPFs in Well Y1 show a very small fracture spacing of approximately 1−3 cm, and the fracture passes through the whole core and makes the core disc-like (Figs. 6(a), 6(d)). BPFs in Well Y301 and Y2 have a larger fracture spacing of 4−8 cm, and some of the BPFs only pass through part of the core (Figs. 6(b), 6(c), and 6(e)).

The bedding structures in sandstones of the study area are mainly parallel-bedding (Figs. 6(b), 6(c), 6(d), and 6(e)) or low angle cross-bedding (Fig. 6(a)). The BPFs are generally parallel to the bedding in the study area.

The vertical distribution of the BPFs shows that they exist in both the Upper Jurassic formation and the Lower Cretaceous formations with similar characteristics. BPFs in Well Y1 Lower Cretaceous show disc thickness of 2−4 cm with no filling.

The number of vertical or high dip-angle fractures is small, which are mainly close to the thrust faults (Fig. 1(c)). Wells, such as Wells Y301 and Y7, all show a few vertical/high dip-angle fractures (Figs. 6(b) and 6(e)).

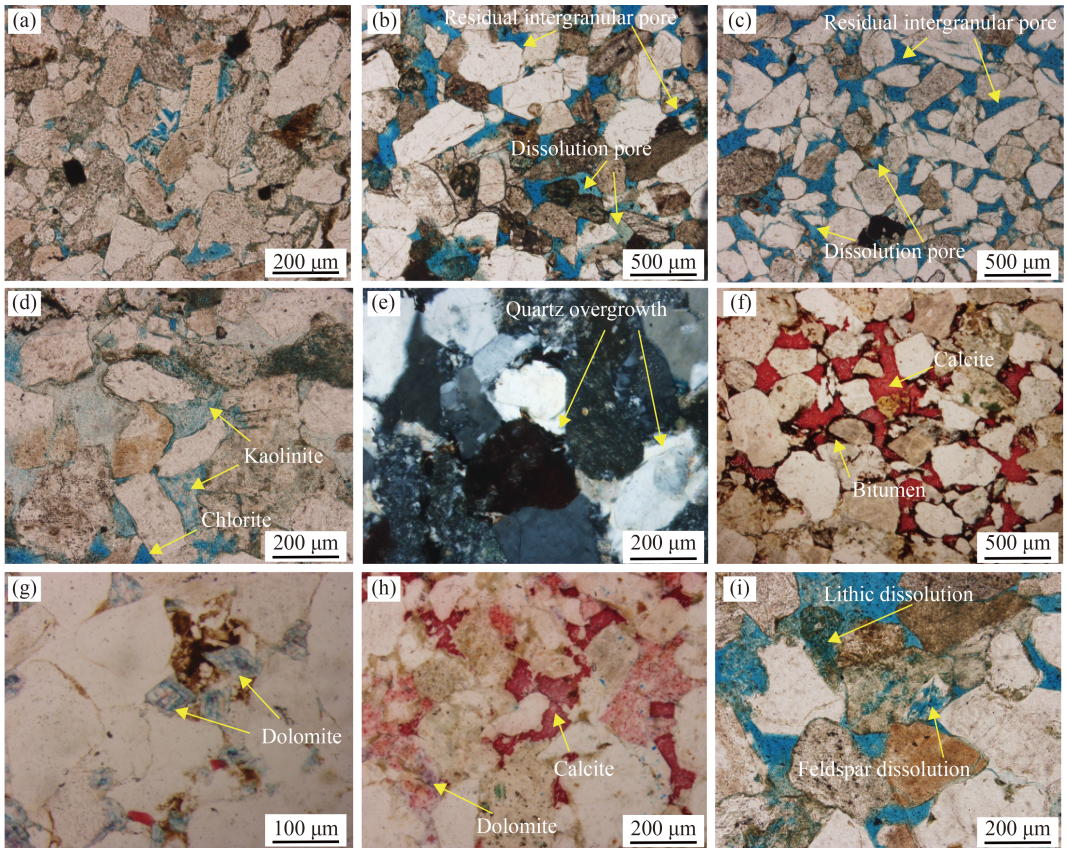

Fig. 5 Photography of blue epoxy resin-impregnated thin sections illustrates the diagenetic types. (a) Intensive compaction with line contact, Well Y1, 5826.65 m. (b) Line-point contact sandstone with both residual intergranular pores and dissolution pores, Well Y1, 5821 m. (c) Point-contact sandstone with both residual intergranular pores and dissolution pores, Well Y301, 5549 m. (d) Kaolinite and chlorite cements, Well Y1, 5882 m. (e) Quartz overgrowth, Well Y3, 5619 m. (f) Calcite cements after bitumen charging, Well Y6, 6048.59 m. (g) Dolomite cement in pores with partial dissolution, Well Y6, 6028.52 m. (h) Calcite and dolomite cementation showing calcite and dolomite colors of red and purple using alizarin red, respectively. (i) Lithic and feldspar partial dissolution, Well Y1, 5821 m.

4.3.2 BPFs in thin sections

Core observations were only able to show the macro-occurrence of the BPFs. The thin sections were used to identify the distribution and filling state of the BPFs.

Images of the thin sections were captured parallel to the bedding. Some important characteristics can be obtained.

1) The BPFs are generally parallel to bedding. Thin sections from Wells Y1, Y3, and Y301 all show that the BPFs are parallel to bedding, which is more obvious than those observed in cores (Figs. 7(a), 7(b), and 7(c)).

2) The BPFs are mainly distributed in areas with high porosity, large grain size, and high quartz grain content. Figures 7(a) and 7(b) illustrates that the sections with BPFs all have higher porosities than the surrounding smaller grain size sections. The areas with fine grains show almost no fractures.

3) No cementation can be found in the BPFs. Many of the BPFs in shale are filled by calcite (Cobbold and Rodrigues, 2007; Zanella et al., 2015; Ukar et al., 2017; Su et al., 2022). However, there is no filling cement or bitumen in the study area. The fracture aperture ranges from 1 to 100 μm in the thin sections (Figs. 7(c) and 7(d)).

4) The BPFs are mainly tensile fractures. Shear fractures and tensile fractures usually show different occurrences. Shear fractures are mostly continuous, and there are displacements in the shear direction. However, the tensile fractures are discontinuous and only displace in the vertical direction. Most BPFs in Figs. 7(a), 7(b), and 7(c) do not pass through the single grains and usually end at the edge of the grains. The BPFs with large apertures also only have a displacement in the vertical direction with almost no displacements in the horizontal direction. One characteristic that should also be noted is that the BPFs cut the quartz overgrowths (Fig. 7(c)), which indicates that the fractures formed after the quartz overgrowths.

4.3.3 Element geochemistry of the BPF surface

The BPF surface element geochemistry can be obtained using a hand-held element analyzer, which is more convenient than laboratory analysis. A few BPF surfaces and fresh core surfaces were analyzed to determine

Fig. 6 Photography of the cores with different fracture types. (a) Bedding-parallel fractures (BPFs) (core discing) in the Qigu Formation, Well Y1. (b) Bedding-parallel fractures (core discing) and vertical fractures in the Qigu Formation, Well Y301. (c) and (d) Bedding-parallel fractures in the Qigu Formation, Well Y2. (e) Bedding parallel fractures (BPFs) in Qigu Formation, Well Y2. (f) High dip-angle fractures in the Qigu Formation, Well Y7.

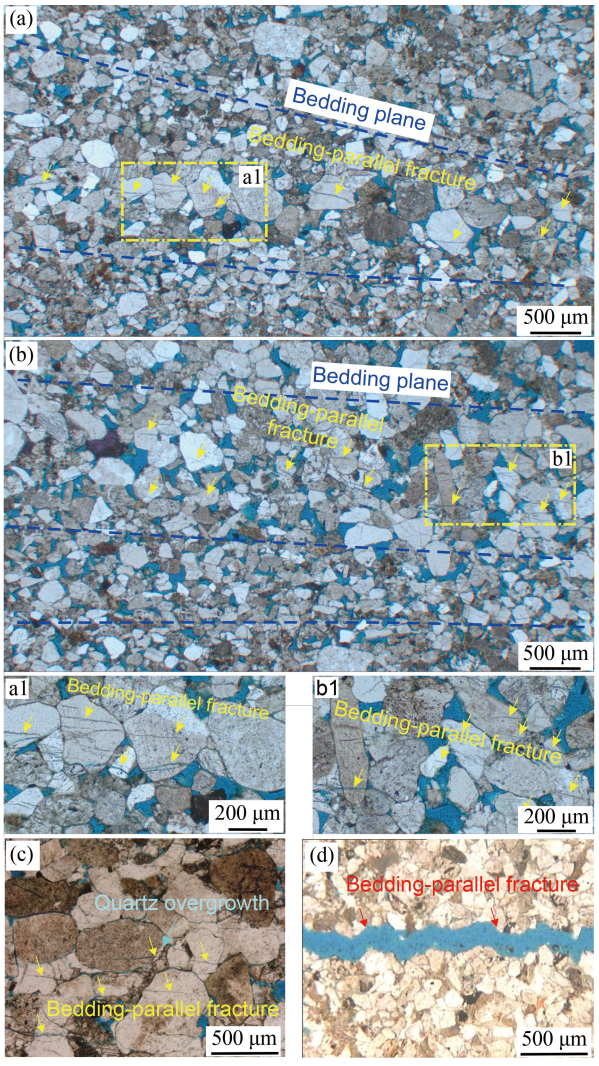

Fig. 7 Photography of blue epoxy resin-impregnated thin sections illustrating the bedding-parallel fractures. (a) Bedding-parallel fractures in coarse grains, Qigu Formation, Well Y301, 5549.2 m. Section a1 is magnified to show the pore-filling state of the BPFs. (b) Bedding-parallel fractures in coarse grains, Qigu Formation, Well Y301, 5544.7 m. Section b1 is magnified to show the pore-filling state of the BPFs. (c) Bedding-parallel fractures in coarse grains that pass through quartz overgrowths, Qigu Formation, Well Y1, 5827.7 m. (d) Bedding-parallel fractures in tight rocks. No horizontal displacement, filling, or dissolution in the fracture. Qigu Formation, Well Y3, 5865.6 m.

whether there was any cement on the fracture surface. Many studies on fractures show that there is calcite or quartz on the natural fracture surfaces (Luo et al., 2020). The element geochemistry analysis of BPF surfaces and fresh surfaces of cores are given in Fig. 8.

The results show that the Ca mass contents of BPF surfaces and fresh core surfaces are very similar, ranging from 2.56% to 2.97%. The main difference between the BPF surface and the fresh surface is the mass content of Ba and S, which were caused by the invasion of oil-based drilling mud. The analysis indicates that the BPF surfaces do not have calcite cement even on the fractures that pass through the cores.

4.3.4 BPFs and reservoir quality

Exploration history shows that almost all wells with high oil production show high BPF densities (He et al., 2011). Statistics of the reservoir quality with BPFs and without BPFs are given in Fig. 9. The porosities of rocks with BPFs are mainly higher than 7%, and the permeabilities are higher than 0.3 mD, which are generally higher than those of rocks without BPFs. The samples with BPFs are limited due to the core discing of the rock, which makes it difficult to obtain standard rock samples for porosity and permeability analysis.

4.3.5 BPFs and faults

Tectonic-related fractures are mainly close to faults, and

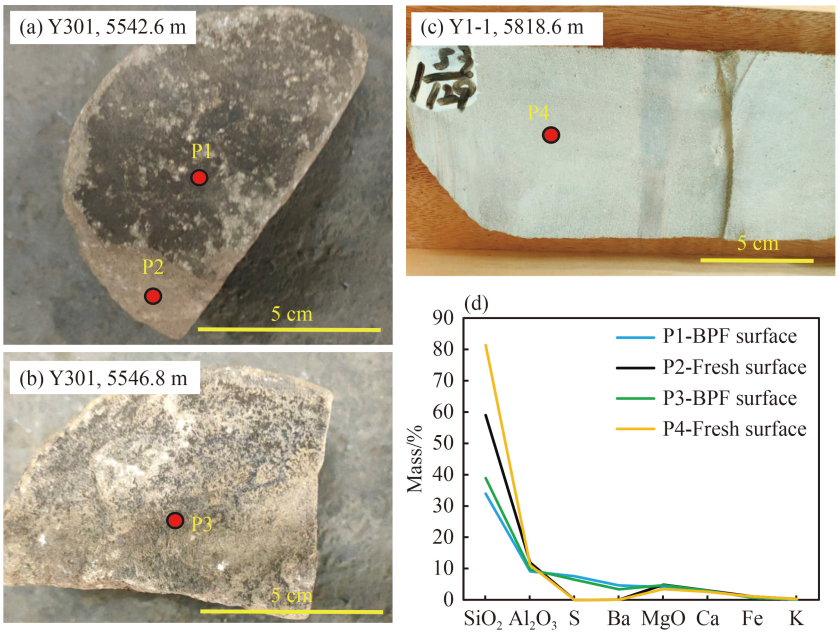

Fig. 8 Bedding-parallel fracture surface (P1, P3) and fresh surface (P2, P4) element geochemistry analysis using the portable element analyzer. (a), (b), and (c) are the cores used for the element geochemistry analysis and (d) is the element mass content. Ba and S elements are the main difference between BPF surfaces and fresh surfaces. The Ba and S come from the invasion of the oil drilling mud.

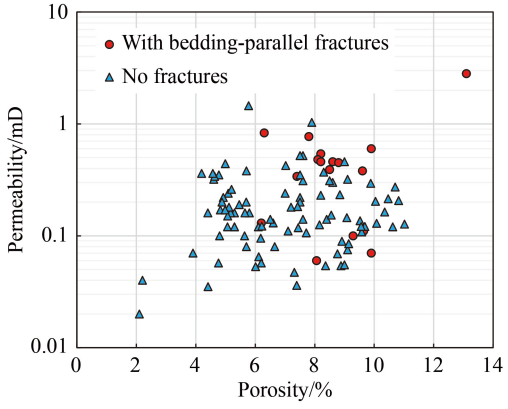

Fig. 9 Porosity and permeability cross-plot with and without bedding-parallel fractures. Samples with bedding-parallel fractures display higher porosity and permeability.

the relationship between fractures and faults could be a good indicator of their origin. BPF development in different wells in Qigu Formation is given in Fig. 10. The cored wells with a high BPF density include Wells Y1, Y3, and Y301 in the study area. Well Y3 is far from the faults but shows a high BPF density. Both BPFs and vertical fractures exist in Well Y301. Other cored wells, such as Wells Y6, Y7, Y12, and Y302, show no BPFs and no oil production. Vertical/high dip-angle fractures are also developed in Wells Y6 and Y7. The relationship between the BPFs, vertical/high dip-angle fracture development, and the faults indicate BPFs may not be related to the thrust faults, whereas the vertical/high dip-angle fractures are developed close to the faults.

4.4 Oxygen and carbon stable isotope geochemistry

Carbonate cement is the main cement in the study area, which may be used to analyze oxygen and carbon stable isotope geochemistry. Oxygen and carbon stable isotope data indicate the origin of carbonate precipitation and temperature during precipitation. The time of carbonate cement preservation may be used to infer the time of fracture development.

The $\delta^{13}C$ value (VPDB) of carbonate cement ranges from −19.07% to −1.98% with an average of −6.91%. The $\delta^{18}O$ value (VPDB) ranges from −21.28% to −11.62%, with an average of −16.67% (Fig. 11(a)). The $\delta^{13}C$ and $\delta^{18}O$ value cross-plots indicate that much of the carbon resulted from the decarboxylation of organic matter.

The calculated oxygen isotope precipitation temperature shows a large range from 69.5°C to 149.6°C (Fig. 11(b)), which indicates that carbonate cement formed from the early diagenetic stage to the middle diagenetic stage. The distribution of oxygen isotope temperature shows a temperature distribution in two groups, one ranging from 80°C to 110°C and another from 110°C to 130°C.

5 Discussion

5.1 Timing of the BPFs

The timing of the BPFs can be determined from either the

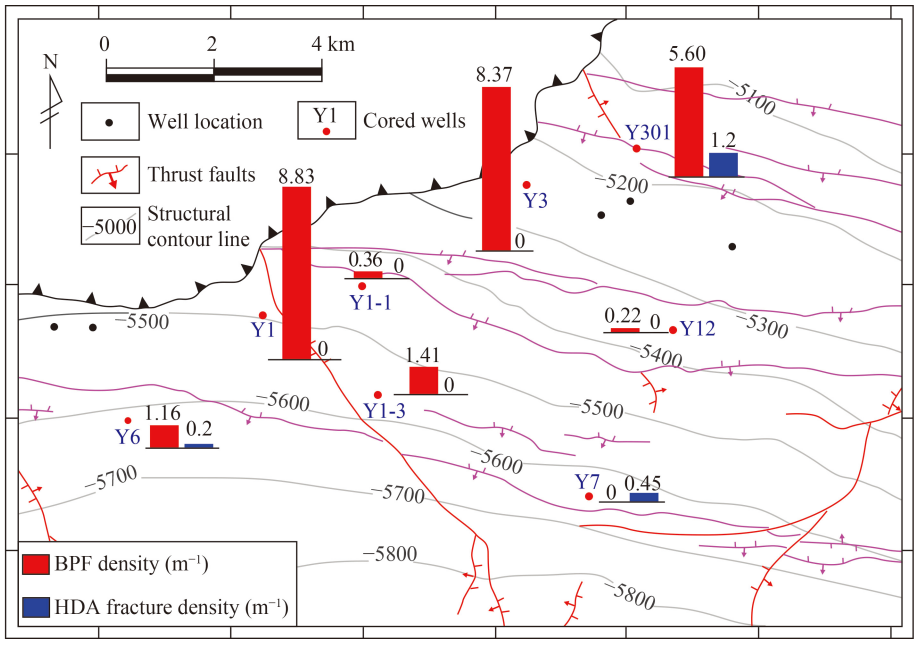

Fig. 10 Bedding-parallel fracture (BPF) density and high dip-angle fracture (HDA) density with respect to the faults on the top of Jurassic formation. The wells with high BPF density can be either close to faults or far from faults. The HDA fractures are mainly close to the faults.

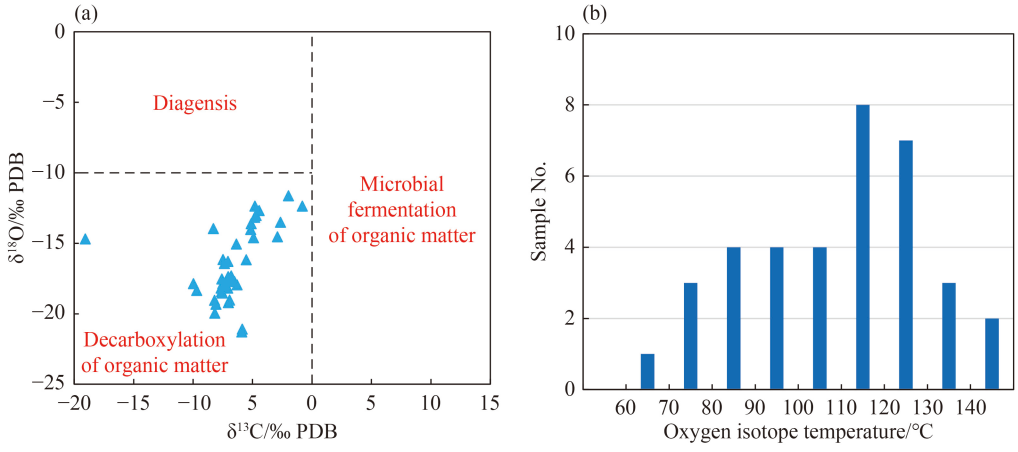

Fig. 11 (a) The $\delta^{13}C$ and $\delta^{18}O$ values of calcite cement in tight sandstones of the Qigu Formation. (b) Histogram of the oxygen isotope temperature distribution in tight sandstones of the Qigu Formation.

cutting relationship between the fractures of different stages (Zeng et al., 2007) or the fracture-filling minerals (Zanella et al., 2015; Zhang et al., 2016; Wang et al., 2020; Su et al., 2022). Core observations, thin section analysis, and fracture surface geochemistry analysis all show that the fractures are without cementation, which makes it difficult to constrain the time of BPF development. The main evidence that can be used to determine the BPF timing includes the following.

1) The vertical distribution of BPFs. Previous studies have linked the formation of BPFs to uplift and thrust fault development in the Late Jurassic, and the overpressure maintained the open BPFs (He et al., 2011). However, core observations show that BPFs were discovered not only in the Upper Jurassic formations but also in the Lower Cretaceous, which indicates that the BPFs formed after the Early Cretaceous.

2) The formation of carbonate cements and the filling state of fractures. The oxygen isotope-calculated temperature ranges from 69.5°C to 149.6°C, with the main precipitation temperature from 80°C to 140°C. Previous studies also analyzed the formation temperature of the calcite and dolomite, with calcite precipitation at 90°C to 120°C (Xi et al., 2019) and dolomite formed later than calcite. The pore-filling characteristics of calcite and dolomite are different. Calcite is preserved as poikilitic cement, and dolomite occurs as automorphic granular cement in the pores. We may infer that if the BPFs formed before the calcite cement, then the BPFs should be filled by calcite. However, thin section observations

show that the BPFs are unfilled. Therefore, the BPFs are possibly formed after the carbonate cements, especially after the massive calcite cementation. When carbonate cement precipitation temperature is placed on the burial history map, the formation time can be determined. Figure 12 shows the burial history of Well Y1 (Shi et al., 2009) and the carbonate cementation time. BPFs should have formed after the middle Cretaceous or even later than the late Paleogene.

5.2 Origin of the core discing

Previous studies have provided many mechanisms for the formation of BPFs in tight sandstone reservoirs. The origins include ① diagenetic origin, ② tectonic origin, ③ overpressure caused by oil/gas generation, ④ natural hydraulic fracturing, ⑤ acidic fluid dissolution, and ⑥ tensile fractures while drilling under high *in situ* stress conditions. A diagenetic origin means that BPFs formed under compaction, pre-solution, and shrinkage during diagenetic processes (Luo et al., 2017; Ju et al., 2020; Zeng et al., 2022). The tectonic origin emphasizes the effect of tectonic compression on the rocks and the fractures formed at the weak surfaces, such as the bedding surfaces (Zeng et al., 2009; Ju et al., 2020). Overpressure-induced BPFs are mainly a result of oil and gas generation that leads to tensile fractures in the horizontal direction (Cobbold and Rodrigues, 2007; Cobbold et al., 2013; Zanella et al., 2015). Natural hydraulic fracturing is similar to the overpressure effect but emphasizes fluid injection after oil and gas accumulation (Wu et al., 2003; Ju et al., 2020). The acidic fluid dissolution origin mainly stresses the effect of acidic fluid injection and dissolution of the grains at the bedding surfaces.

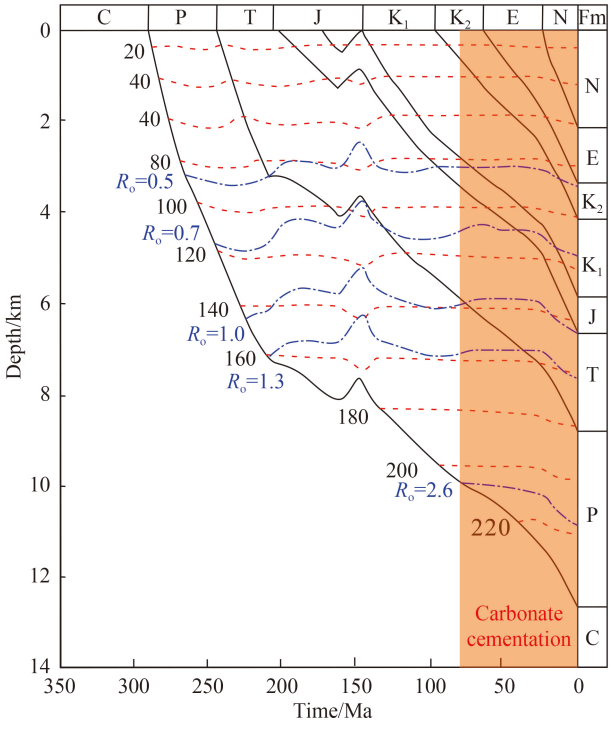

Fig. 12 Burial history of Well Y1 and the carbonate cementation formation time. Bedding-parallel fractures should have formed after the carbonate cements (Modified from Shi et al. (2009)).

Apart from the BPF origins listed above, geotechnical engineers have also observed BPFs or core discing due to tensile breakage at the time of drilling in areas with high *in situ* horizontal stresses (Jaeger and Cook, 1963; Obert and Stephenson, 1965; Hou, 1985; Lim and Martin, 2010; Zheng et al., 2020). Core discing rocks have been widely discovered in different lithologies, such as sandstone, granite, and marble, which were mainly discovered at hydropower stations (Lim and Martin, 2010; Zheng et al., 2020). There was no oil/gas injection in these rocks, but they had high *in situ* horizontal stresses. Many numerical simulations have also shown the formation of tensile fractures at the time of well drilling (Belov and Ivanov, 1993; Wu et al., 2018; Zheng et al., 2020).

The lack of scratches or horizontal displacements and the discontinuous nature of BPFs in cores and thin sections indicate that the BPFs are not typical shear fractures but are more likely to be tensile fractures. Therefore, the BPFs are unlikely to have formed by tectonic compression and thrust faults. The relationship between BPFs distribution and thrust faults (Fig. 10) indicates that faults are not the main controlling factor.

The tensile fractures may have been induced by the overpressure caused by oil/gas injection, natural hydraulic fracturing, or drilling. Zanella et al. (2015) pointed out that once the pore pressure exceeds the overburden stress, the vertical effective stress may become tensile and may form BPFs. Previous studies have shown that the overpressure in the Yongjin Oil Field was caused by gas generation after the early Neogene (Shi et al., 2009). Overpressure began in the late Paleogene and reached its peak during the present. The present measured pore pressure coefficient ranges from 1.6 to 1.87, which is very high. However, if the average density is given a value of 2.2 g/cm^3, depth of 6000 m, and pressure coefficient of 1.87, the overburden stress is still larger than the pore pressure, with values of 132 MPa and 112.2 MPa, respectively. Therefore, overpressure is not the main mechanism of BPF formation.

Natural hydraulic fracturing may be caused by the oil-charging process. However, oil charging may result in the preservation of bitumen and the dissolution of grains. Ju et al. (2020) pointed out that the origin of BPFs in the Yanchang Formation in the Ordos Basin was due to the joint effects of overpressure and tectonic compression. Since the overpressure in the Ordos Basin resulted from oil injection, most fracture surfaces are filled by bitumen (Fig. 13) (Ju et al., 2020; Zeng et al., 2022). We may infer that natural hydraulic fracturing is also not the main controlling factor for BPF formation in our study area.

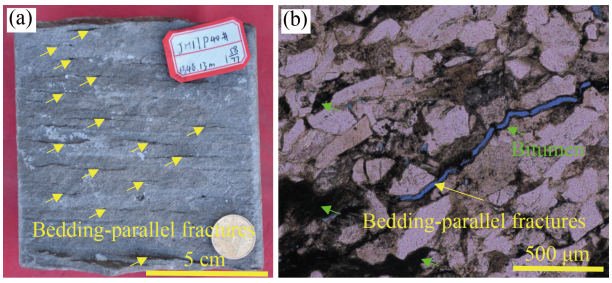

Fig. 13 Bedding-parallel fractures in (a) core and (b) thin sections in the Yanchang Formation in the Ordos Basin, China. The fractures were filled by bitumen, which was jointly affected by the overpressure and tectonic compression.

In the study area, the BPF formation mechanisms of tight sandstones suggested by petroleum geologists are all excluded. The mechanism raised by geotechnical engineers should be considered as the potential mechanism.

Figure 14 shows the formation mechanism of core discing during drilling. The mechanism can be divided into two processes: core crack propagation and breaking into discs. The drilling activities result in the adjustment of the local stress field. The borehole is subjected to radial compression and axial tension. Stress concentration tends to occur at the core roots, which are in contact with the crown surface of a drill bit (Li et al., 2004; Shi et al., 2019). Core cracks start to propagate when the stress concentration reaches the rock failure strength. The crack propagation will lead to stress concentration at the crack tip, which may finally separate from the surrounding rock. As the drill continues in a downward direction, the same cycle will repeat again and form the core discing phenomenon.

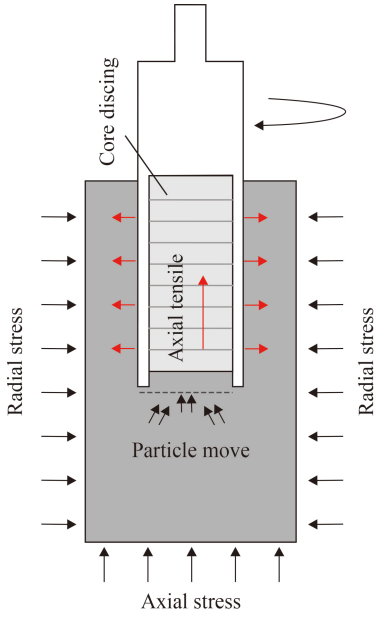

Fig. 14 Core discing formation mechanisms during drilling (modified from Zheng et al. (2020)).

The controlling factors for disc thickness have also been widely discussed (Hou, 1985; Zhou, 2020; Huang et al., 2020). The key factors controlling the disc thickness (t) include the maximum horizontal stress (σ_1), the diameter of the core (D), and the tensile strength (σ_t). Figure 15 shows the cross-plot of the disc thickness and horizontal stress with different tensile strengths at the Ertan Hydropower Station, Sichuan, China (Hou, 1985). The results show that the disc thickness decreases with increasing maximum horizontal stress. High tensile strength also results in thick core disc.

The well-logging calculated maximum horizontal stress, which is constrained by hydraulic fracturing experiments, ranges from 150 to 170 MPa in the Upper Jurassic formation. The tensile strength ranges from 10 to 25 MPa, and the core diameter is approximately 15 cm. The calculated disc thickness mainly ranges from 0.75 to 1.5 cm when we use the plate in Fig. 15. Core observations show that disc thickness in the study area mainly ranges from 1 to 8 cm, which is larger than the calculated values. We may infer that this difference is mainly caused by the different in situ stress environments between the two areas and the bedding structure in sedimentary rocks.

From the thin sections and core observations, we may also infer that the BPFs mainly occur in rocks with good reservoir quality. Reservoirs with good reservoir quality have small tensile strengths that may lead to thin core discs. In the sedimentary rocks, the breakages mainly exist on the bedding surface grains, which are weaker and more brittle than the surrounding grains (Figs. 7(a) and 7(b)). This is the main reason why all wells with high oil production show high BPF densities in core observation. The BPFs in the study area may not be the main fluid flow zones but may be an indicator of good reservoir quality. The existence of BPFs makes it difficult to obtain samples for porosity and permeability measurements. However, the high facial porosity and low clay content in

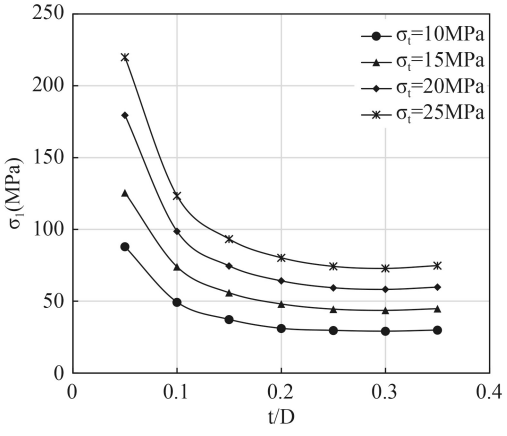

Fig. 15 The relationship among core disc thickness (t/D), horizontal maximum *in situ* stresses (σ_1), and tensile strengths (σ_t) in rocks from Ertan Hydropower Station, Sichuan, China (Hou, 1985).

the rocks with BPFs indicate that the high oil production rate is a result of the good reservoir quality but not the bedding-parallel fractures.

6 Conclusions

This study focuses on the characteristics of the bedding-parallel fractures in the ultradeep tight sandstone reservoir in the Yongjin Oil Field, Junggar Basin, China. The origins of the BPFs are also examined. The main conclusions are as follows.

1) The bedding-parallel fractures in the study area are parallel to the bedding structures planes, which show low dip angle with the core radial direction. BPFs can either pass through part the core or split into discs, with similar thickness of 1−8 cm. Core and microscopic observation show that the BPFs are unfilled, discontinuous, and with no bitumen or grain dissolution, which indicates that the BPFs are tensile fractures.

2) The BPFs can be discovered in tight sandstone reservoirs with relatively high porosity and permeability in both Upper Jurassic and Lower Cretaceous formations. They can be discovered either close to the faults or far from the faults.

3) The presence of BPFs in both Upper Jurassic and Lower Cretaceous formations indicates that the fractures were developed later than the early Cretaceous. No carbonate cements, bitumen filling and no grain dissolution indicate that the BPFs were formed later than the oil charging and carbonate cementation period. Oxygen and carbon stable isotope analysis shows that the carbonate cements are formed after the middle Cretaceous and continue to exist until present.

4) The BPFs were tensile fractures, which were most likely to be generated from core drilling under high *in situ* stress conditions. In sedimentary rocks, the BPFs mainly formed at the bedding surfaces. Reservoirs with better reservoir quality tend to have smaller tensile strengths and smaller fracture spacing. The existence of a high BPF density is an indicator of good reservoir quality and may result in high oil production.

Acknowledgments This research is jointly financed by the National Natural Science Foundation of China (Grant Nos. 41902147, 42130813, and 41402117) and the Shengli Geophysical Research Institute of Sinopec. We thank the useful discussions with Dr. Tao Wen and Dr. Yankun Wang on the origins of the BPFs. We also thank the editors and the reviewers for the carefully review and constructive comments.

References

Belov N I, Ivanov V I (1993). Numerical modeling of the stressed state of the foot of a borehole with a study of drill core disking. J Min Sci, 28(6): 500–503

Bian W, Hornung J, Liu Z, Wang P, Hinderer M (2010). Sedimentary and palaeoenvironmental evolution of the Junggar Basin, Xinjiang, northwest China. Palaeobio Palaeoenv, 90(3): 175–186

Cobbold P R, Rodrigues N (2007). Seepage forces, important factors in the formation of horizontal hydraulic fractures and bedding-parallel fibrous veins ('beef' and 'cone-in-cone'). Geofluids, 7(3): 313–322

Cobbold P R, Zanella A, Rodrigues N, Løseth H (2013). Bedding-parallel fibrous veins (beef and cone-in-cone): worldwide occurrence and possible significance in terms of fluid overpressure, hydrocarbon generation and mineralization. Mar Pet Geol, 43: 1–20

Flottmann T, Campagna D J, Hillis R, Warner D (2004). Horizontal microfractures and core discing in sandstone reservoirs, Cooper Basin, Australia. In: PESA Eastern Australasian basins symposium II, Adelaide: 2004

He Z J, Liu B J, Wang P (2011). Genesis of bedding fracture and its influences on reservoirs in Jurassic, Yongjin area, Junggar Basin. Petrol Geol Recov Eff, 18(1): 15–17 (in Chinese)

Hou F L (1985). Critical ground stress of core discing and the relation between thickness of rock core and ground stress. J Wuhan Inst Hydr Elec Eng, 1: 37–48 (in Chinese)

Hu H Y, Li P P, Wang G J (2008). Mechanism of secondary porosity development of Xishanyao Formation (J2x) in Yongjin Block, Junggar Basin. Geol Sci Technol Info, 27(3): 21–25 (in Chinese)

Hu X W, Yang X Y, Ren Y S, Wu Z J, Du G F, Huang T T (2020). Sedimentary environment and tectonic evolution of Junggar Basin: constrains on the mineralization of sandstone-type uranium deposits. Geotectonica et Metallogenia, 44(4): 725–741 (in Chinese)

Huang H X, Lv Y R, Cai Y (2020). Interval fracturing of unloading rock-columns and disking mechanisms of rock cores. Chinese J Rock Mech Eng, 39(5): 1005−1010 (in Chinese)

Jaeger J C, Cook N G W (1963). Pinching-off and disking of rocks. J Geophys Res, 68(6): 1759–1765

Ju W, You Y, Feng S B, Xu H R, Zhang X L, Wang S Y (2020). Characteristics and genesis of bedding-parallel fractures in tight sandstone reservoirs of Chang 7 oil layer, Ordos Basin. Oil Gas Geol, 41(03): 596–605

Lai J, Liu B, Li H, Pang X, Liu S, Bao M, Wang G (2021). Bedding parallel fractures in fine-grained sedimentary rocks: recognition, formation mechanisms, and prediction using well log. Petrol Sci, 19(2): 554−569

Li C, Zhao L, Liu B, Liu H, Li J, Fan Z, Wang J, Li W, Zhao W, Sun M (2021). Origin, distribution and implications on production of bedding-parallel fractures: a case study from the Carboniferous KT-I Formation in the NT oilfield, Precaspian Basin, Kazakhstan. J Petrol Sci Eng, 196: 107655

Li S S, Nie D X, Ren G M (2004). The fracture mechanism of discal drill core and its influence on characteristic of engineering geology. Adv Earth Sci, 19(S1): 384–387

Lim S S, Martin C D (2010). Core disking and its relationship with stress magnitude for Lac du Bonnet granite. Int J Rock Mech Min Sci, 47(2): 254–264

Liu H, Luo Y, Meng Y, Xiao G, Zhao Y, Zhou S, Shao L (2021). Effects of pore structure on the moveable oil saturation in water-driven tight oil sandstone reservoirs. J Petrol Sci Eng, 207: 109142

Liu H, Zhao Y, Luo Y, Xiao G, Meng Y, Zhou S, Shao L (2020).

Origin of the reservoir quality difference between Chang 8 and Chang 9 Member sandstones in the Honghe Oil Field of the Southern Ordos Basin, China. J Petrol Sci Eng, 185: 106668

Luo Q, Wei H Y, Liu D D, Zhang C, Zhu D, Zhang Y, Wang J (2017). Research significance, advances and trends on the role of bedding fracture in tight oil accumulation. Petrol Geol Exp, 39(1): 1–7 (in Chinese)

Luo Y, Wang Y, Liu H, Wang G, Zhao Y (2020). Overpressure controlling factors for tectonic fractures in near-source tight reservoirs in the southwest Ordos Basin, China. J Petrol Sci Eng, 188: 106818

Obert L, Stephenson D E (1965). Stress conditions under which core discing occurs. SME Trans, 232(3): 227–235

Qu G S, Ma Z J, Chen X F, Li T, Zhang N (2009). On structures and evolutions in Junggar Basin. Xinjiang Petrol Geol, 30(1): 1–5

Shi J N, Zou H Y, Li P P, Liu J Z (2009). Analysis of main controlling factors for hydrocarbon accumulation in Yongjin region of Junggar Basin. J China Univ Min Technol, 38: 384–389

Shi Y P, Xia Y M, Tan Q, Zhang Y C, Qiao S (2019). Distribution of contact loads in crushed zone between tunnel boring machine disc cutter and rock. J Cent South Univ, 26(9): 2393–2403

Su A, Bons P D, Chen H, Feng Y X, Zhao J X, Song J (2022). Age, material source, and formation mechanism of bedding-parallel calcite beef veins: case from the mature Eocene lacustrine shales in the Biyang Sag, Nanxiang Basin, China. Geol Soc Am Bull, 134(7−8): 1811−1833

Ukar E, Lopez R G, Gale J F, Laubach S E, Manceda R (2017). New type of kinematic indicator in bed-parallel veins, Late Jurassic–Early Cretaceous Vaca Muerta Formation, Argentina: EW shortening during Late Cretaceous vein opening. J Struct Geol, 104: 31–47

Wang M, Chen Y, Bain W M, Song G, Liu K, Zhou Z, Steele-MacInnis M (2020). Direct evidence for fluid overpressure during hydrocarbon generation and expulsion from organic-rich shales. Geology, 48(4): 374–378

Wu S, Wu H, Kemeny J (2018). Three-dimensional discrete element method simulation of core disking. Acta Geophys, 66(3): 267–282

Wu Z J, Tang H J, An F S (2003). Causes of bedding fractures of tight sand gas-reservoir in Xinchang, West Sichuan region. Pet Explor Dev, 30(2): 109–111

Xi K, Cao Y, Liu K, Wu S, Yuan G, Zhu R, Zhou Y, Hellevang H (2019). Geochemical constraints on the origins of calcite cements and their impacts on reservoir heterogeneities: a case study on tight oil sandstones of the Upper Triassic Yanchang Formation, southwestern Ordos Basin, China. AAPG Bull, 103(10): 2447–2485

Yang Z (2009). Hydrocarbon accumulation mechanisms near the top overpressured surface in central Junggar Basin, northwest China. Dissertation for the Doctoral Degree. Wuhan: China University of Geoscience

Yang Z, Wang J H, Lin S H, Wu S T, Liu Y, Li Q Y, Zhang P Z (2011). Hydrocarbon accumulation mechanism near top overpressured surface in central Junggar Basin. J China Univ Petrol, 35(3): 19–26

Zanella A, Cobbold P R, Boassen T (2015). Natural hydraulic fractures in the Wessex Basin, SW England: widespread distribution, composition and history. Mar Pet Geol, 68: 438–448

Zeng L B, Li Z X, Shi C E, Wang Z G, Zhao J Y, Wang Y K (2007). Characteristics and origin of fractures in the extra low-permeability sandstone reservoirs of the Upper Triassic Yanchang Formation in the Ordos Basin. Acta Geol Sin, 81(2): 174–180

Zeng L B, Lyu W Y, Xu X, Tian H, Lu S L, Zhang M J (2022). Development characteristics, formation mechanism and hydrocarbon significance of bedding fractures in typical tight sandstone and shale. Acta Petrol Sin, 43(2): 180–191

Zeng L B, Wang Z G, Xiao S R, Zhang G B (2009). The origin and geological significance of low dip angle fractures in the thrust zones of the western basins of China. Acta Petrol Sin, 30(1): 56–60

Zhang J F, Lan C L (2006). Fractures and faults distribution and its effect on gas enrichment areas in Ordos Basin. Pet Explor Dev, 33(2): 172−177 (in Chinese)

Zhang J, Jiang Z, Jiang X, Wang S, Liang C, Wu M (2016). Oil generation induces sparry calcite formation in lacustrine mudrock, Eocene of east China. Mar Pet Geol, 71: 344–359

Zheng M Z, Li S J, Yao Z, Zhang A D, Xu D P, Zhou J F (2020). Core discing characteristics and mitigation approach by a novel developed drill bit in deep rocks. J Cent South Univ, 27(10): 2822–2833

Zhou J F (2020). Relationship between rock core-discing and geostress in Jinping underground laboratory. Soil Eng Found, 34(6): 706−710 (in Chinese)